Immunity, Volume *54*

Supplemental information

Live imaging of SARS-CoV-2 infection in mice reveals that neutralizing antibodies require Fc function for optimal efficacy

Irfan Ullah, Jérémie Prévost, Mark S. Ladinsky, Helen Stone, Maolin Lu, Sai Priya Anand, Guillaume Beaudoin-Bussières, Kelly Symmes, Mehdi Benlarbi, Shilei Ding, Romain Gasser, Corby Fink, Yaozong Chen, Alexandra Tauzin, Guillaume Goyette, Catherine Bourassa, Halima Medjahed, Matthias Mack, Kunho Chung, Craig B. Wilen, Gregory A. Dekaban, Jimmy D. Dikeakos, Emily A. Bruce, Daniel E. Kaufmann, Leonidas Stamatatos, Andrew T. McGuire, Jonathan Richard, Marzena Pazgier, Pamela J. Bjorkman, Walther Mothes, Andrés Finzi, Priti Kumar, and Pradeep D. Uchil

Figure S1

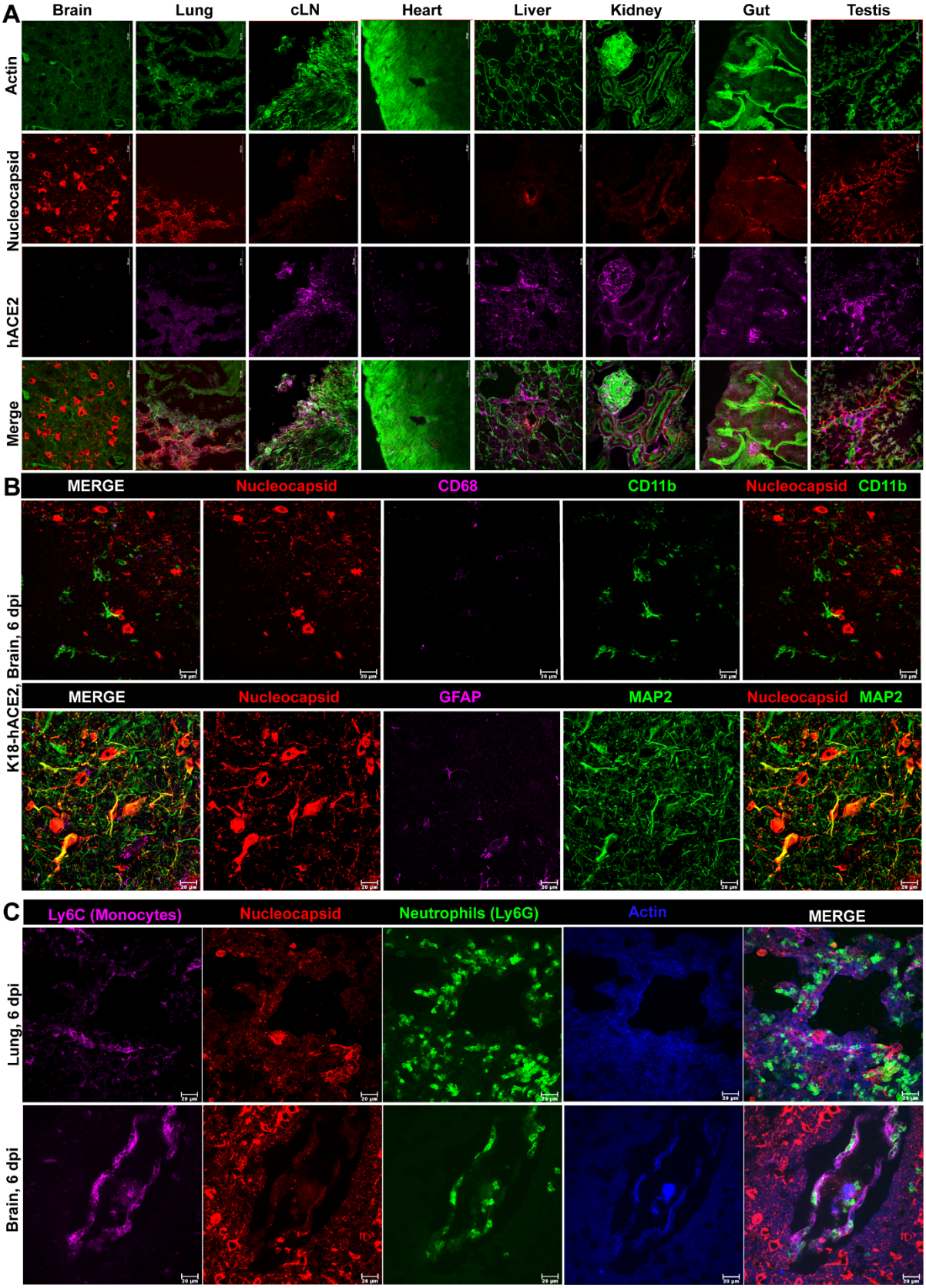
A
Brain
Lung
cLN
Heart
Liver
Kidney
Gut
Testis
Actin
Nucleocapsid
hACE2
Merge
B
MERGE
Nucleocapsid
CD68
CD11b
Nucleocapsid CD11b
K18-hACE2, Brain, 6 dpi
MERGE
Nucleocapsid
GFAP
MAP2
Nucleocapsid MAP2
C
Ly6C (Monocytes)
Nucleocapsid
Neutrophils (Ly6G)
Actin
MERGE
Lung, 6 dpi
Brain, 6 dpi

Figure S1. SARS-CoV-2-nLuc Replicates and Disseminates to Multiple Tissues in K18-hACE2 Mice. Related to Figure 1.

(A) Images of cryosections from indicated tissues of SARS-CoV-2-nLuc infected K18-hACE2 mouse harvested at 6 dpi. Actin (green), nucleocapsid (red) and hACE2 (magenta) were detected using phalloidin and respective antibodies. Notably, hACE2 appeared as puncta on the surface of infected neurons and lung tissue compared to other organs where the signal was more uniform and stained a region of the cell surface. Scale bar: 50 μm

(B) Images of cryosections from brain tissues of SARS-CoV-2-nLuc infected K18-hACE2 mouse harvested at 6 dpi to characterize infected cells. Glial cells (top panel) were identified using antibodies to markers CD68 (magenta) and CD11b (green). Neurons (lower panel) were identified using antibodies to MAP2 (green) and mature astrocytes were identified using antibodies to GFAP (magenta). SARS-CoV-2 infected cells were identified using antibodies to nucleocapsid (red). Nucleocapsid positive cells were predominantly positive for MAP2. Scale bar: 20 μm

(C) Images of cryosections from lung and brain tissues of SARS-CoV-2-nLuc infected K18-hACE2 mouse harvested at 6 dpi to visualize neutrophil and inflammatory monocyte infiltration. Monocytes and neutrophils were identified using antibodies to markers Ly6C (magenta) and Ly6G (green) respectively. SARS-CoV-2 infected cells were identified using antibodies to nucleocapsid (red) and actin (blue) was stained using phalloidin conjugated to AF_{405}. Scale bar: 20 μm. A-C are representative images from n=4 mice per group.

Figure S2

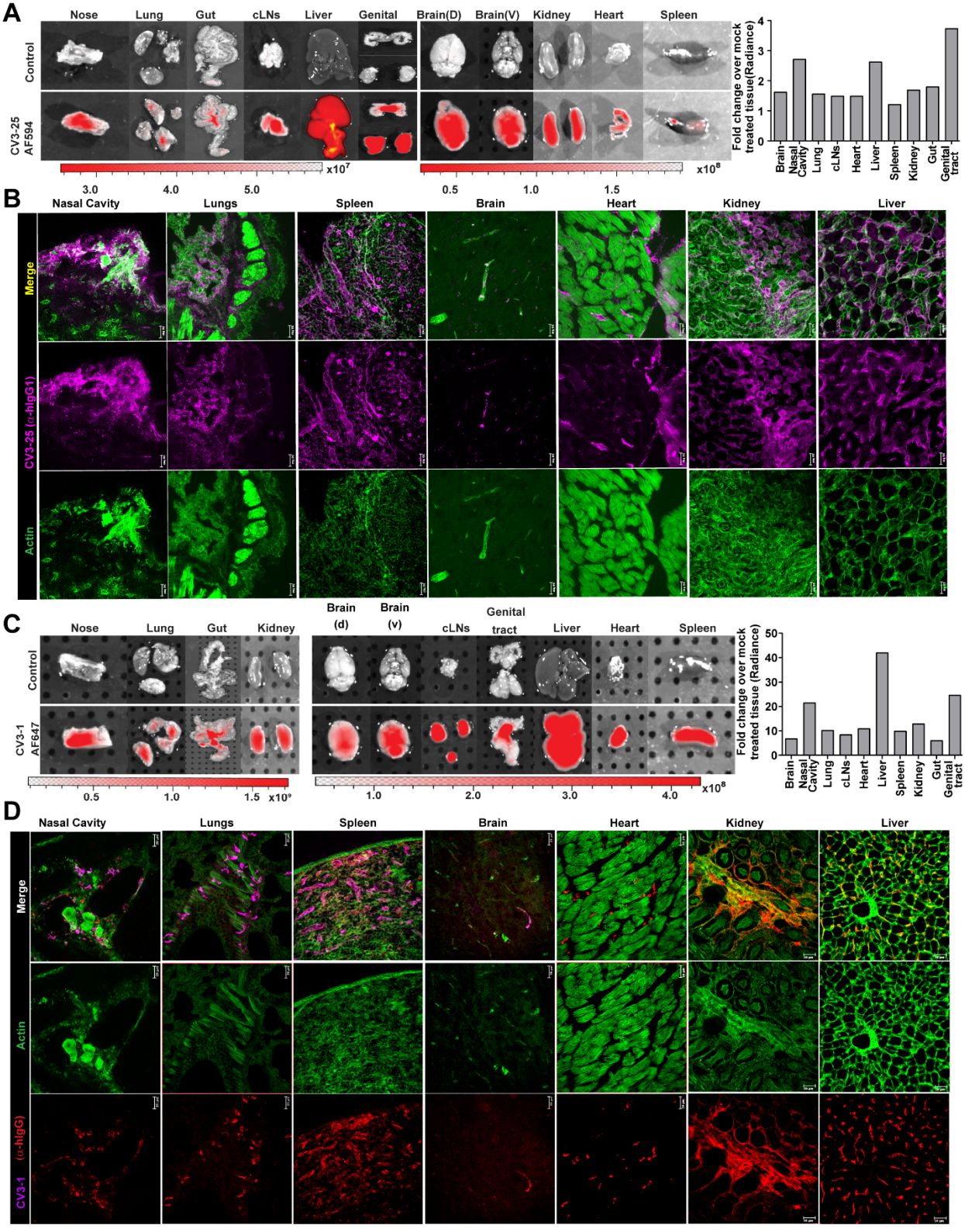
A
Nose
Lung
Gut
cLNs
Liver
Genital
Brain(D)
Brain(V)
Kidney
Heart
Spleen
Control
CV3-25 AF594
x10^7
x10^8
Fold change over mock treated tissue(Radiance)
Brain
Nasal Cavity
Lung
cLNs
Heart
Liver
Spleen
Kidney
Gut
Genital tract
B
Nasal Cavity
Lungs
Spleen
Brain
Heart
Kidney
Liver
Merge
CV3-25 (α-higG1)
Actin
C
Nose
Lung
Gut
Kidney
Brain (d)
Brain (v)
cLNs
Genital tract
Liver
Heart
Spleen
Control
CV3-1 AF647
x10^9
x10^8
Fold change over mock treated tissue (Radiance)
D
Nasal Cavity
Lungs
Spleen
Brain
Heart
Kidney
Liver
Merge
Actin
CV3-1 (α-higG)

Figure S2. *Ex vivo* Imaging and Immunostaining of Tissues Reveal Widespread Biodistribution of CV3-25 and CV3-1 NAbs in Mice 24 h After Intraperitoneal Delivery. Related to Figure 3.

(A) C57BL/6J mice were either mock treated (PBS) or intraperitoneally administered 12.5 mg/kg body weight of CV3-25 monoclonal antibody conjugated to Alexa Fluor 594 (CV3-25 AF_{594}). 24 h later, indicated tissues were imaged using the fluorescence module in IVIS spectrum to detect AF_{594}. The plot shows the quantified radiance detected in indicated tissues after normalization with corresponding organs from control mouse.

(B) Images of cryosections from indicated tissues from CV3-25 AF_{594}-treated mouse as in A. Actin and CV3-25 were detected using phalloidin-AF_{488} and AF_{647} conjugated anti-human IgG respectively. Scale bar: 20 μm

(C) C57BL/6J mice were either mock treated (PBS) or intraperitoneally administered 12.5 mg/kg of CV3-1 monoclonal antibody conjugated to Alexa Fluor 647 (CV3-1 AF_{647}). 24 h later, indicated tissues were imaged using the fluorescence module in IVIS spectrum to detect AF_{647}. The plot shows the quantified radiance detected in indicated tissues after normalization with corresponding organs from control mouse.

(B) Images of cryosections from indicated tissues from CV3-1 AF_{647}-treated mouse as in A. Actin was detected using phalloidin-AF_{488}. CV3-1 AF_{647} was detected in the red channel using Alexa Fluor 568 conjugated anti-human IgG. Scale bar: 20 μm

Data in panels B-K are from one to two independent experiment n= 1 per group

Figure S3

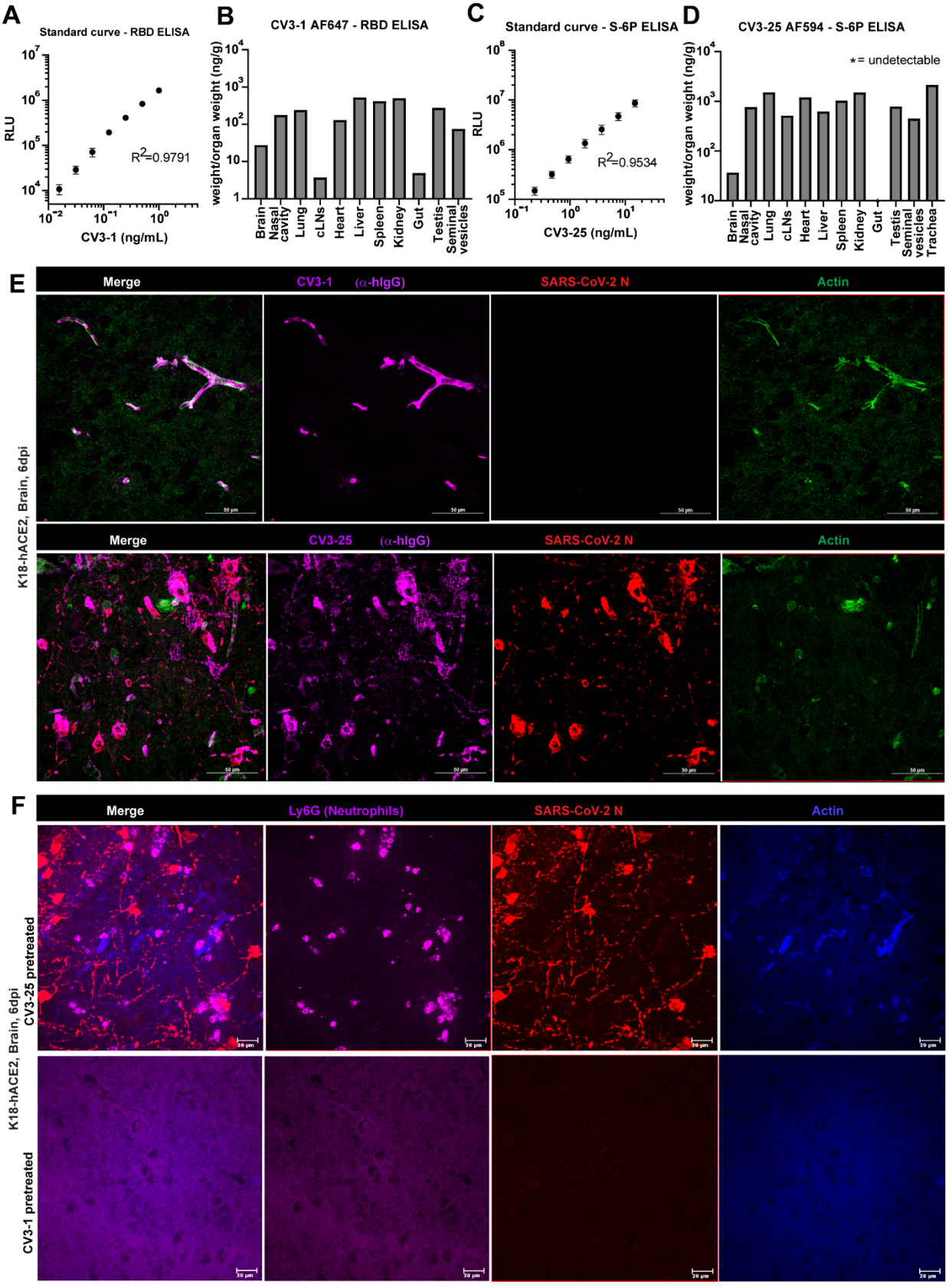
A
Standard curve - RBD ELISA
RLU
CV3-1 (ng/mL)
R2=0.9791
B
CV3-1 AF647 - RBD ELISA
weight/organ weight (ng/g)
Brain
Nasal cavity
Lung
cLNs
Heart
Liver
Spleen
Kidney
Gut
Testis
Seminal vesicles
C
Standard curve - S-6P ELISA
RLU
CV3-25 (ng/mL)
R2=0.9534
D
CV3-25 AF594 - S-6P ELISA
*= undetectable
weight/organ weight (ng/g)
Brain
Nasal cavity
Lung
cLNs
Heart
Liver
Spleen
Kidney
Gut
Testis
Seminal vesicles
Trachea
E
Merge
CV3-1 (α-hIgG)
SARS-CoV-2 N
Actin
K18-hACE2, Brain, 6dpi
Merge
CV3-25 (α-hIgG)
SARS-CoV-2 N
Actin
F
Merge
Ly6G (Neutrophils)
SARS-CoV-2 N
Actin
K18-hACE2, Brain, 6dpi
CV3-25 pretreated
CV3-1 pretreated

Figure S3. Quantitative ELISA of Tissue Homogenates Ascertains Widespread Biodistribution of CV3-1 and CV3-25 NAbs in Mice. Related to Figure 4.

(A-D) Estimation of CV3-25 and CV3-1 NAbs biodistribution in mice using ELISA. Measurement of anti-Spike NAbs concentration in organs was performed using quantitative ELISA. (A-B) Recombinant SARS-CoV-2 RBD and (C-D) S-6P proteins were used to quantify CV3-1 and CV3-25 antibody concentration, respectively. Linear standard curves using known concentrations of CV3-1 or CV3-25 NAbs were established for inferring the antibody concentration in organ homogenates. Serial dilutions of homogenized mice organs were prepared in PBS and incubate on antigen-coated plates. The presence of anti-Spike NAbs was revealed using HRP-conjugated anti-human IgG secondary Abs. The signal obtained with BSA (negative control) was subtracted for each organ. Relative light unit (RLU) values were transformed into a NAb concentrations based on the standard curve and the dilution factor. Subsequently, these concentration values were multiplied with the homogenization volume and divided by the total organ weight.

(E) Persistence and redistribution of neutralizing NAbs in SARS-CoV-2 infected mice. Images of brain tissue from K18-hACE2 mice infected with SARS-CoV-2-nLuc at 6 dpi that were prophylactically treated with CV3-1 or CV3-25 (12.5 mg/kg body weight), 24 h before infection. Actin (green) was labelled using phalloidin, CV3-1 and CV3-25 (magenta) were detected using anti-hIgG conjugated to AF_{647} and infected cells (red) were identified using antibodies to SARS-CoV-2 N. CV3-1 localizes to the endothelial walls of blood vessels and CV3-25 redistributes to decorate infected neurons in addition to endothelium (seen in UI mice; Figure S2). Scale bar: 50 μm

(F) Assessment of neutrophil infiltration in the brains of CV3-25 and CV3-1-pretreated mice for an experiment as in E. Neutrophils were identified using antibodies to marker Ly6G (magenta) and SARS-CoV-2 infected cells were identified using antibodies to nucleocapsid (red) and actin (blue) was stained using phalloidin conjugated to AF_{405}. Scale bar: 20 μm.

Results shown in (A-D) were obtained from organs harvested from one mouse per antibody and E-F are representative images from n=4 mice per group.

Figure S4

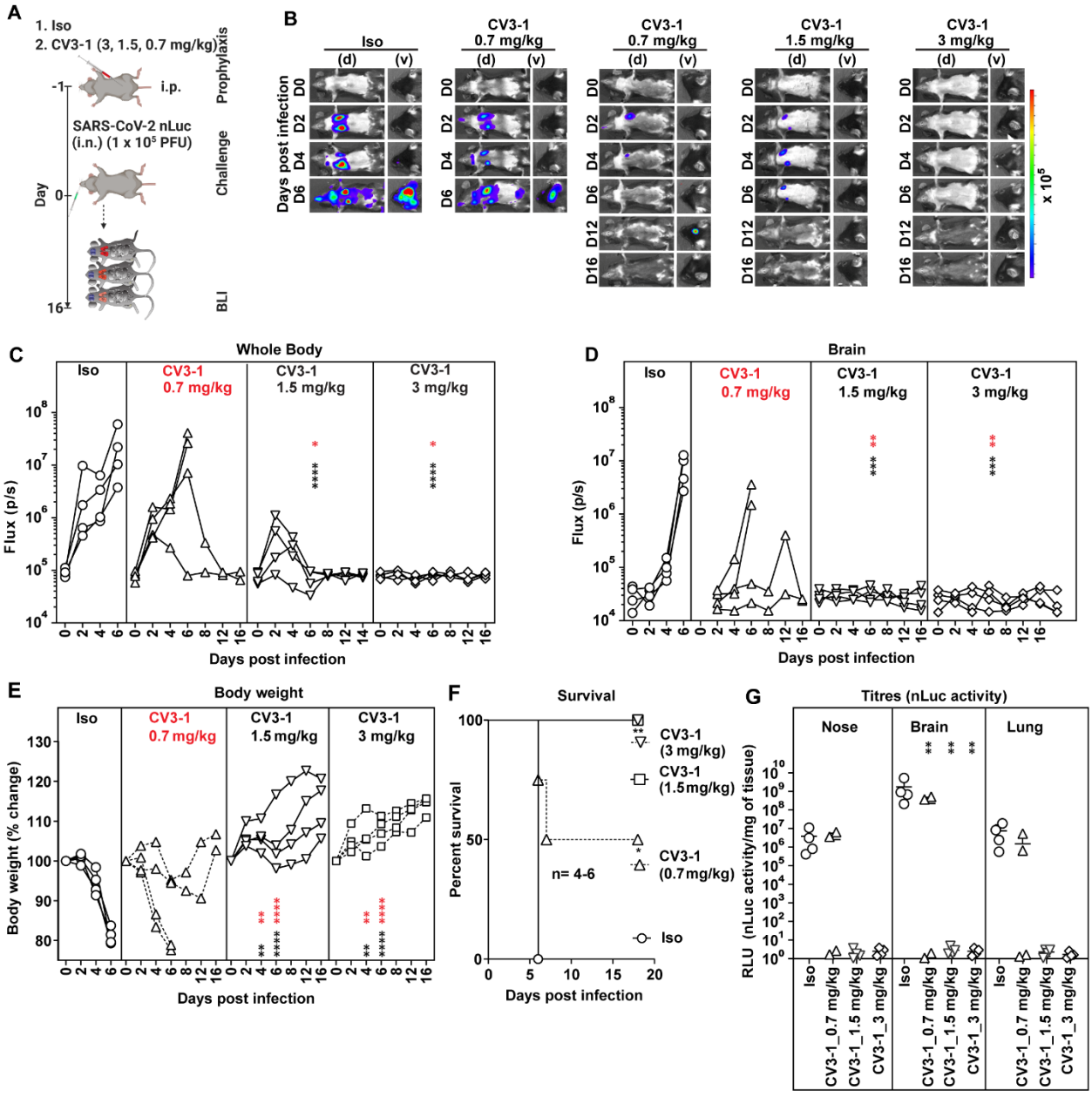

Figure S4. CV3-1 attains Prophylactic EC_{50} at 0.7 mg/kg Dose in K18-hACE2 Mice. Related to Figure 4.

(A) A scheme showing experimental design for testing the dose of CV3-1 NAb to achieve protection for lethal SARS-CoV-2-nLuc infection. Indicated concentration of CV3-1 NAb was delivered (i.p.) 1 day before challenging K18-hACE2 mice (n = 4-6 per group; two independent experiments) with 1 x 10^5 FFU of SARS-CoV-2 nLuc. Human IgG1-treated (12.5 mg/kg) mice were used as control (isotype treated). Mice were followed by non-invasive BLI every 2 days from

the start of infection using IVIS Spectrum after retroorbital administration of furimazine (nLuc substrate).

(B) SARS-CoV-2 replication and dissemination in K18-hACE2 transgenic mice for experiment as in A, were monitored via BLI in ventral (v) and dorsal (d) positions at the indicated days post infection every 2 days. Images from two mice under CV3-1 prophylaxis (0.7 mg/kg) are shown where one mouse succumbed at 6 dpi and the other survived despite weak but observable neuroinvasion. Images from one representative experiment are shown for the rest.

(C-D) A plot showing temporal quantification of nLuc signal acquired non-invasively and displayed as photon flux (photons/sec) in whole body or brain region of SARS-CoV2-nLuc infected K18-hACE2 mice for an experiment as in A. Each curve represents luminescent signal computed for individual mouse. Scale bars denote radiance in photons per second per square centimeter per steradian (p/sec/cm2/sr).

(E) A plot showing temporal body weight changes in indicated groups of K18-hACE2 mice at indicated days post infection for an experiment shown in A. Each curve represents one animal. The body weight at the start of the experiment was set to 100 %.

(F) Kaplan-Meier survival curves of mice statistically compared by log-rank (Mantel-Cox) test for experiment as in A.

(G) Plot showing viral loads as nLuc activity/mg of indicated organs using Vero E6 cells as targets. Undetectable virus amounts were set to 1 for display on log plots.

Grouped data in (C)-(E) and G were analyzed by 2-way ANOVA followed by Dunnett's or Tukey's multiple comparison tests. Statistical significance: group comparisons to isotype control are shown in black; group comparisons to CV3-1 (0.7 mg/kg) are shown in red. $*$, $p < 0.05$; $**$, $p < 0.01$; $***$, $p < 0.001$; $****$, $p < 0.0001$; Mean values ± SD are depicted.

Figure S5

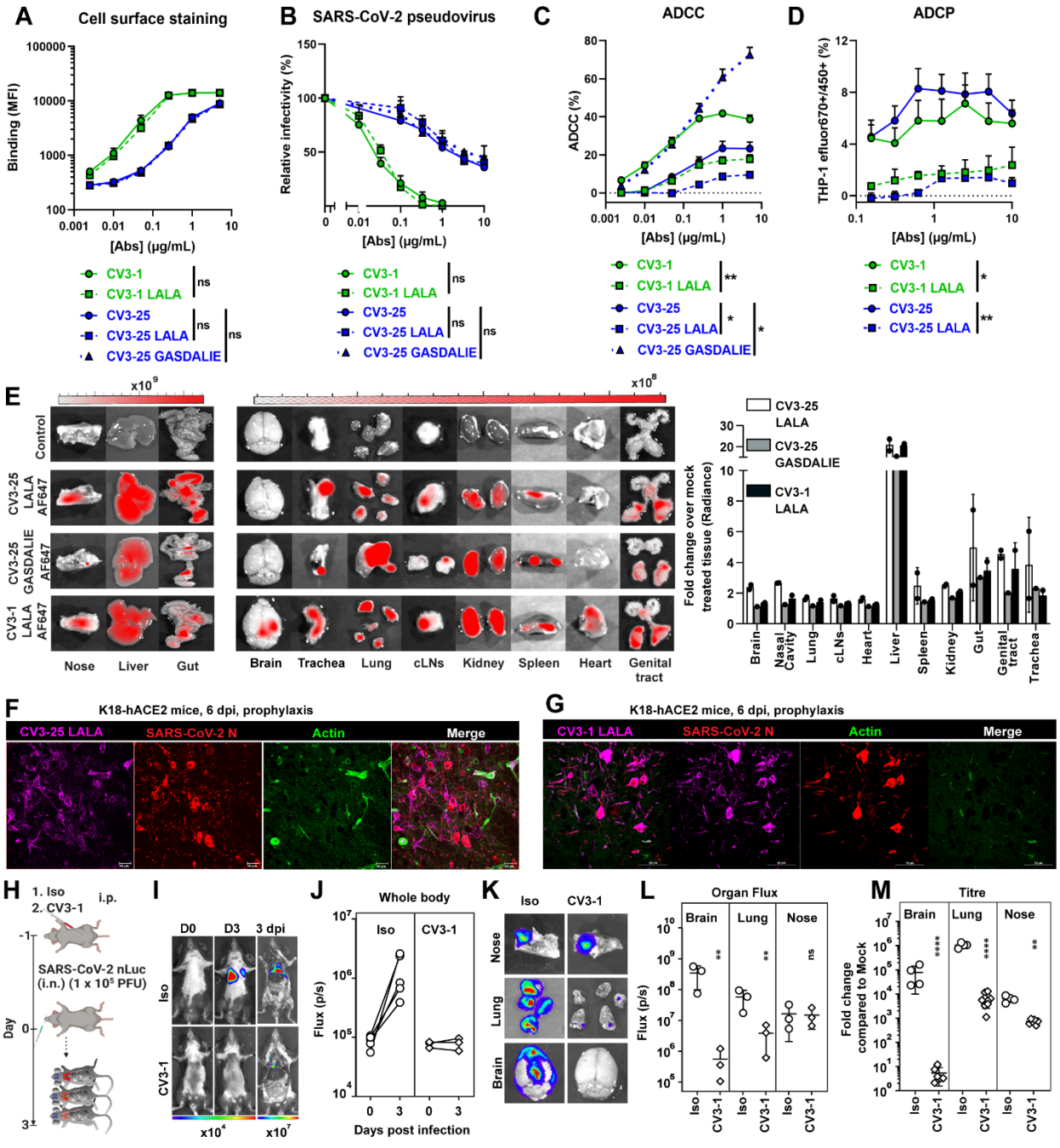

Figure S5. LALA Mutations Diminish and GASDALIE Mutations Enhance Antibody Effector Functions of NAbs without Compromising Neutralizing Activity. Related to Figure 6.

(A) Cell-surface staining of CEM.NKr cells stably expressing full-length SARS-CoV-2 Spike (CEM.NKr-Spike) using CV3-1 and CV3-25 mAbs or their LALA and GASDALIE mutant counterparts. The graph shown represent the mean fluorescence intensities (MFI)

obtained. with titrated concentrations of anti-Spike NAbs. MFI values obtained with parental CEM.NKr were subtracted.

(B) Pseudoviral particles encoding for the luciferase reporter gene and bearing the SARS-CoV-2 S glycoproteins were used to infect 293T-ACE2 cells. Neutralizing activity was measured by incubating pseudoviruses with titrated concentrations of anti-Spike NAbs at 37°C for 1 h prior to infection of 293T-ACE2 cells. Neutralization half maximal inhibitory antibody concentration (IC_{50}) values were determined using a normalized non-linear regression using GraphPad Prism software.

(C) Using a FACS-based ADCC assay, CEM.NKr parental cells were mixed at a 1:1 ratio with CEM.NKr-Spike cells and were used as target cells. PBMCs from uninfected donors were used as effector cells. The graph shown represent the percentages of ADCC obtained in the presence of titrated concentrations of anti-Spike NAbs.

(D) Using a FACS-based ADCP assay, CEM.NKr-Spike cells were used as target cells and THP-1 monocytic cell line was used as effector cells. The graph shown represent the percentages of effector cells that had phagocytosed target cells obtained in the presence of titrated concentrations of anti-Spike NAbs. Statistical significance was tested using a non-parametric Mann-Whitney test for pairwise comparison between WT and LALA NAbs (*, $p < 0.05$; **, $p < 0.01$; ns, not significant)

(E-F) Biodistribution of LALA and GASDALIE mutants of indicated NAbs in mice 24 h after i.p. delivery (n=1-2 per group; one to two independent experiments). B6 mice were either isotype treated (control) or intraperitoneally administered of Alexa Fluor 647 conjugated NAb mutants (12.5 mg/kg body weight). 24 h later, indicated tissues were imaged using the fluorescence module in IVIS spectrum to detect Alexa Flour 647. The plot shows the quantified radiance detected in indicated tissues after normalization with corresponding organs from control mouse.

(G, H) Images of cryosections from brain tissues of K18-hACE2 mice pretreated with LALA mutants of CV3-25 or CV3-1 (i.p., 12.5 mg/g body weight) at 6 dpi. Actin was detected using phalloidin-Alexa Fluor 488. CV3-25 and CV3-1 (magenta) were detected using Alexa Fluor 647 conjugated anti-human IgG respectively. Infected cells were detected using antibodies to SARS-CoV-2 nucleocapsid (red). Images show penetration of both CV3-25 and CV3-1 NAbs into the brain and localization to the surface of infected neurons. Scale bar: 20 μm

(I) SARS-CoV-2 can establish infection in nasal cavity and lungs during CV3-1 prophylaxis. A scheme showing experimental design to test establishment of virus infection in K18-hACE2 mice (n = 4 per group from one independent experiment) pretreated with CV3-1 NAb (i.p.,12.5 mg/kg body weight), 1 day before challenging with 1×10^5 FFU of SARS-CoV-2 nLuc. Mice treated

similarly with Isotype matched hIgG1 were used as controls. The mice were followed by non-invasive BLI at 0 and 3 dpi using IVIS Spectrum after retroorbital administration of furimazine (nLuc substrate).

(J) SARS-CoV-2 replication and dissemination in indicated groups of K18-hACE2 transgenic mice for experiment as in I, were monitored via BLI at the indicated times. The mice were euthanized at 3 dpi and imaged again after necropsy. Images from one representative experiment are shown.

(K) A plot showing temporal quantification of nLuc signal acquired non-invasively and displayed as photon flux (photons/sec) in whole body of SARS-CoV2-nLuc infected K18-hACE2 mice for an experiment as in I. Each line represents luminescent signal computed for individual mouse.

(L, M) *Ex vivo* imaging of indicated organs after necropsy at 3 dpi and quantification of nLuc signal displayed as photon flux (photons/sec) in K18-ACE2 mice for experiment as in I.

(N) A plot showing real-time PCR analyses to detect SARS-CoV-2 nucleocapsid (N) gene mRNA in indicated organs of K18-hACE2 mice after necropsy for an experiment as in I. The data were normalized to *Gapdh* mRNA in the same sample and that in non-infected mice.

Results shown (A-D) were obtained in at least three independent experiments. Scale bars denote radiance (photons/sec/cm^2/steradian). *p* values obtained by non-parametric Mann-Whitney test for pairwise comparison with isotype-treated controls; *, $p < 0.05$; **, $p < 0.01$; ***, $p < 0.001$; ****, $p < 0.0001$; individual data points along with mean values ± SD are depicted.

Figure S6

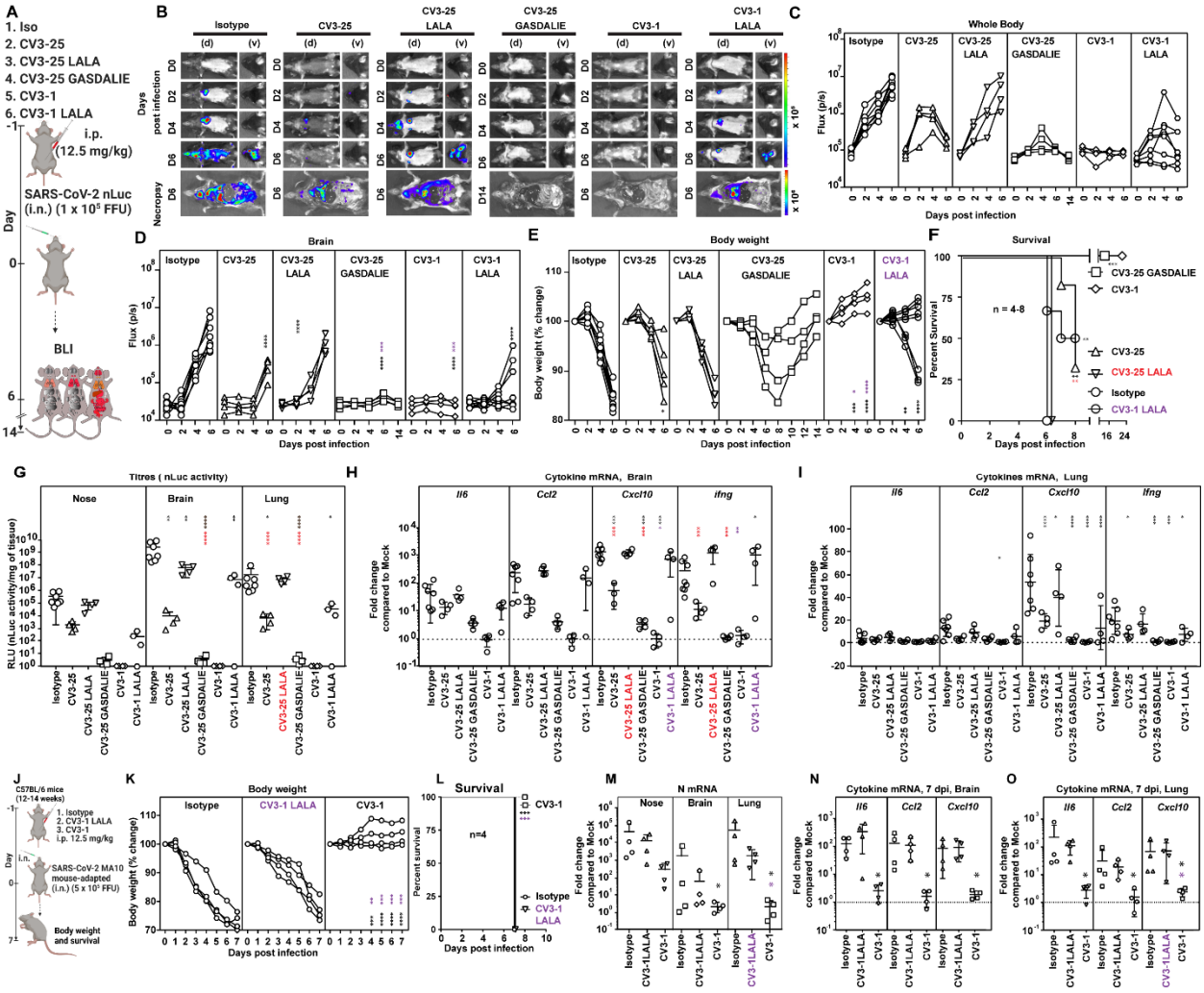

Figure S6. Fc-mediated Antibody Effector Functions Contribute to *In Vivo* Efficacy of CV3-1 and CV3-25 During Prophylaxis. Related to Figure 6.

(A) A scheme showing experimental design for testing *in vivo* efficacy of NAbs and their corresponding Leucine to Alanine (LALA) or G236A/S239D/A330L/I332E (GASDALIE) mutants (12.5 mg/kg body weight) delivered intraperitoneally (i.p.) 1 day before challenging K18-hACE2 mice (n = 4-8 per group; two independent experiments) with 1 x 10^5 FFU of SARS-CoV-2 nLuc. Human IgG1-treated (12.5 mg/kg body weight) mice were used as control (Iso). Mice were followed by non-invasive BLI every 2 days from the start of infection using IVIS Spectrum after retroorbital administration of furimazine (nLuc substrate).

(B) SARS-CoV-2 replication and dissemination in K18-hACE2 transgenic mice for experiment as in A, were monitored via BLI in ventral (v) and dorsal (d) positions at the indicated days post

infection every 2 days. The mice were euthanized on indicated days and imaged again after necropsy. Images from one representative experiment are shown.

(C-D) A plot showing temporal quantification of nLuc signal acquired non-invasively and displayed as Flux (photons/sec) in whole body or brain region of SARS-CoV2-nLuc infected K18-hACE2 mice for an experiment as in A. Each curve represents luminescent signal computed for individual mouse.

(E) A plot showing temporal body weight changes of K18-hACE2 mice at indicated days post infection for an experiment shown in A. Each curve represents one animal. The body weight at the start of the experiment was set to 100%.

(F) Kaplan-Meier survival curves of mice statistically compared by log-rank (Mantel-Cox) test for experiment as in A.

(G) Plot showing viral loads as nLuc activity/mg of indicated organs using Vero E6 cells as targets. Nluc activity was determined 24 h after infection for experiment as in A. Undetectable virus amounts were set to 1 for display on log plots.

(H, I) A plot showing mRNA expression of indicated cytokines from lung and brain tissues of K18-hACE2 mice at the time of euthanasia as shown in F. Data were normalized to *Gapdh* mRNA in the same sample and that in non-infected mice after necropsy.

(J) A scheme showing experimental design for testing *in vivo* efficacy of CV3-1 and its corresponding Leucine to Alanine (LALA) mutant (12.5 mg/kg body weight) delivered intraperitoneally (i.p.) 1 day before challenging 12-14 weeks old C57BL/6 (B6) mice with 5 x 10^5 FFU of mouse-adapted SARS-CoV-2 MA10. Human IgG1-treated (12.5 mg/kg body weight) mice were used as control (Iso) (n=4, one experiment).

(K) A plot showing temporal body weight changes of B6 mice at indicated days post infection for an experiment shown in J. Each curve represents one animal. The body weight at the start of the experiment was set to 100%.

(L) Kaplan-Meier survival curves of mice statistically compared by log-rank (Mantel-Cox) test for experiment as in J.

(M-O) A plot showing fold changes in mRNA expression of SARS-CoV-2 N or indicated cytokines from specified tissues of B6 mice at 7 dpi for an experiment as in J. The data were normalized to *GAPDH* in the same sample and that in non-infected mice after necropsy.

Scale bars in (B) denote radiance (photons/sec/cm2/steradian). Grouped data in (C-E) and (G-I), were analyzed by 2-way ANOVA followed by Dunnett's or Tukey's multiple comparison tests. The data in (K) and (M-O) were analyzed using unpaired Mann-Whitney test. Statistical significance: group comparisons to isotype control are shown in black; group comparisons between CV3-25

LALA to CV3-25 and CV3-25 GASDALIE-treated cohorts are shown in red; group comparison between CV3-1 LALA and CV3-1 treated cohorts are shown in purple. $*$, $p < 0.05$; $**$, $p < 0.01$; $***$, $p < 0.001$; $****$, $p < 0.0001$; Mean values ± SD are depicted.

Figure S7

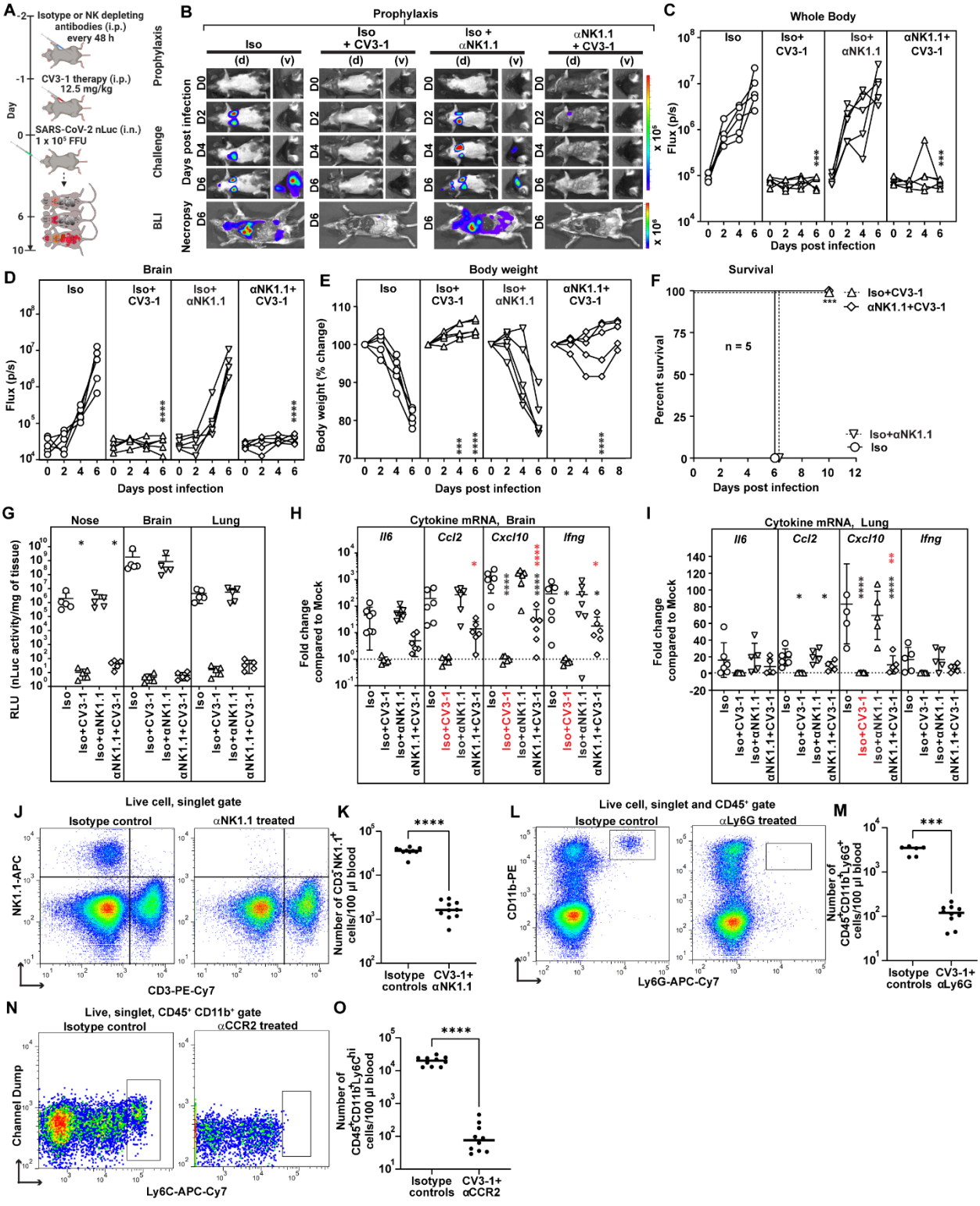
A
Isotype or NK depleting antibodies (i.p.) every 48 h
CV3-1 therapy (i.p.) 12.5 mg/kg
SARS-CoV-2 nLuc (i.n.) 1 x 10⁵ FFU
Day
Prophylaxis
Challenge
BLI
B
Prophylaxis
Iso
Iso + CV3-1
Iso + αNK1.1
αNK1.1 + CV3-1
(d)
(v)
Days post infection
Necropsy
C
Whole Body
Flux (p/s)
Days post infection
D
Brain
E
Body weight
Body weight (% change)
F
Survival
Percent survival
n = 5
Iso+CV3-1
αNK1.1+CV3-1
Iso+αNK1.1
Iso
G
Nose
Brain
Lung
RLU (nLuc activity/mg of tissue)
H
Cytokine mRNA, Brain
Il6
Ccl2
Cxcl10
Ifng
Fold change compared to Mock
I
Cytokine mRNA, Lung
J
Live cell, singlet gate
Isotype control
αNK1.1 treated
NK1.1-APC
CD3-PE-Cy7
K
Number of CD3⁻NK1.1⁺ cells/100 µl blood
Isotype controls
CV3-1+ αNK1.1
L
Live cell, singlet and CD45⁺ gate
αLy6G treated
CD11b-PE
Ly6G-APC-Cy7
M
Number of CD45⁺CD11b⁺Ly6G⁺ cells/100 µl blood
Isotype controls
CV3-1+ αLy6G
N
Live, singlet, CD45⁺ CD11b⁺ gate
αCCR2 treated
Channel Dump
Ly6C-APC-Cy7
O
Number of CD45⁺CD11b⁺Ly6C^hi cells/100 µl blood
Isotype controls
CV3-1+ αCCR2

Figure S7. NK Cells Contribute Marginally to *In Vivo* Efficacy During CV3-1 Prophylaxis. Related to Figure 7.

(A) A scheme showing experimental design for testing the contribution of NK cells in K18-hACE2 mice (n = 5 per group; 2 independent experiments) pretreated with CV3-1 NAb (i.p.,12.5 mg/kg body weight), 1 day before challenging with 1 x 10^5 FFU of SARS-CoV-2 nLuc. αNK1.1 mAb (i.p., 20 mg/kg body weight) was used to deplete NK cells at indicated time points. Corresponding human (for CV3-1) and rat (for αNK1.1) antibodies served as non-specific isotype controls. The mice were followed by non-invasive BLI every 2 days from the start of infection using IVIS Spectrum after retroorbital administration of furimazine (nLuc substrate).

(B) SARS-CoV-2 replication and dissemination in indicated groups of K18-hACE2 transgenic mice for experiment as in A, were monitored via BLI at ventral (v) and dorsal (d) positions at the indicated days post infection every 2 days. The mice were euthanized at indicated times and imaged again after necropsy. Images from one representative experiment are shown.

(C-D) A plot showing temporal quantification of nLuc signal acquired non-invasively and displayed as photon flux (photons/sec) in whole body or brain region of SARS-CoV2-nLuc infected K18-hACE2 mice for an experiment as in A. Each curve represents luminescent signal computed for individual mouse. Scale bars denote radiance (photons/sec/cm^2/steradian).

(E) A plot showing temporal body weight changes in designated groups of K18-hACE2 mice at indicated days post infection for an experiment shown in A. Each curve represents one animal. The body weight at the start of the experiment was set to 100%.

(F) Kaplan-Meier survival curves of mice statistically compared by log-rank (Mantel-Cox) test for experiment as in A.

(G) Plot showing viral loads as nLuc activity/mg of indicated organs using Vero E6 cells as targets. Nluc activity was determined 24 h after infection for an experiment as in A. Undetectable virus amounts were set to 1 for display on log plots.

(H, I) A plot showing fold changes in mRNA expression of indicated cytokines from lung and brain tissues of K18-hACE2 mice at the time of euthanasia as shown in F. The data were normalized to *Gapdh* mRNA in the same sample and that in non-infected mice after necropsy.

(J, K) Representative FACS plots showing the gating strategy to identify NK cells ($CD3^-NK1.1^+$) (n= 8; two experiments) and quantification to ascertain their depletion in PBMCs of indicated groups of mice.

(L, M) Representative FACS plots showing the gating strategy to identify neutrophils cells ($CD45^+$ $CD11b^+Ly6G^+$) (n= 8; two experiments) and quantification to ascertain their depletion in PBMCs of indicated groups of mice.

(N, O) Representative FACS plots showing the gating strategy to identify Ly6C^{hi} monocytes (n= 10; two experiments) and quantification to ascertain their depletion in PBMCs of indicated groups of mice.

Grouped data in (C)-(E) and (G)-(I) were analyzed by 2-way ANOVA followed by Dunnett's or Tukey's multiple comparison tests. Statistical significance: group comparisons to isotype control are shown in black; group comparisons to Iso^{+}CV3-1 treated cohort are in red. Pairwise comparisons in (K), (M) and (O) were analyzed using non-parametric Mann-Whitney test. $*$, $p < 0.05$; $**$, $p < 0.01$; $***$, $p < 0.001$; $****$, $p < 0.0001$; Mean values ± SD are depicted.

Table S1. A Comparison of SARS-CoV-2 Nucleocapsid (N) and *hACE2* mRNA expression in K18-hACE2 Mice Across Various Organs, Related to Figure 1 and S1

Organs	**Fold increase in GAPDH-normalized mRNA levels in tissues compared to uninfected B6 mice**	
	SARS-CoV-2 N (Mean ± SD) (n=6) (Infected K18-hACE2 mice, 6 dpi) (*p value*)*	**hACE2 (Mean ± SD) (n= 4) (UI K18-hACE2 mice) (*p value)****
Brain	303476.00 (± 27526) *(0.0022)*	353.62 (± 145) *(0.0022)*
Lung	2383.07 (± 2666) *(0.0022)*	1131.08 (± 415) *(0.0022)*
Nose	6081.23 (± 5577) *(0.0022)*	518.60 (± 390) *(0.0022)*
cLNs	541.27 (± 541) *(0.0022)*	688.96 (± 379) *(0.0022)*
Trachea	218.11 (± 206) *(0.0022)*	375.90 (± 315) *(0.0022)*
Heart	29.50 (± 17) *(0.0022)*	159.56 (± 55) *(0.0022)*
Liver	2.82 (± 1.5) *(0.0087)*	49.46 (± 12) (*0.0022)*
Spleen	11.65 (± 9) *(0.0087)*	19.75 (± 8) *(0.0022)*
Kidney	43.33 (± 21) *(0.0022)*	487.90 (± 254) *(0.0022)*
Gut	30.85 (± 20) *(0.0022)*	320.03 (± 110) *(0.0022)*
Genital tract	936.94 (± 364) *(0.0022)*	724.26 (± 275) *(0.0022)*

* *p* values obtained by non-parametric Mann-Whitney test for pairwise comparison.